Search for Deeply Bound K^-ppn in the ^{4}He(K^-, n) reaction

Suzuki, T.[a] on behalf of E471 collaboration

[a]University of Tokyo, 7-3-1 Hongo, Bunkyo-ku, Tokyo, Japan

We have performed an experiment to search deeply bound K^-ppn system. We finished data taking at the end of October, 2002. We are presently analyzing the data and describe current status, focusing on stopped K^- event selection and tracking of secondary particles.

1 Physics Motivation

Observation of deeply bound mesic state in nucleus can give certain information about local part of strong interaction. It is widely believed that the quark condensation $<\bar{q}|q>$, which is a result of spontaneous chiral-symmetry breaking, is the origin of the major part of the hadron mass. Actually, vector-meson is expected to change its mass in media proportionally to the condensation[1]. In a pure chiral-limit, pseudo-scaler meson should also be massless. Therefore, one may detect meson-mass shift even in normal nucleon density.

For π meson, a series of observations of deeply bound states had been already performed. On the other hand, such experimental information do not exist for strange mesons, and only information of kaonic hydrogen and nucleon scattering exist. In theoretical field, the existence of deeply bound kaonic state has been predicted[2], and experimental search is awaited.

Under such a situation, E471 experimental group performed the search for deeply bound state of K^- in ^{3}He nucleus, as pioneers of this field[3].

2 Experimental Facility and Setup

The experiment has been performed at KEK-PS north counter hall, K5 beam line(Fig. 1). Secondary particles are generated at production target, and we can extract both particles with positive charge, and negative charge, by changing magnet polarity[4]. To stop as much as kaons in thin target(0.75g/cm^2 liquid ^{4}He), a wedge shaped degrader(WSD) has been installed between Q3 and Q4(momentum-dispersive point). It gives 1.5 times

larger number of K^- stopped in the target compared with the case of no WSD, as described in next section.

A conceptual side view of the experimental setup is shown in Fig. 2.

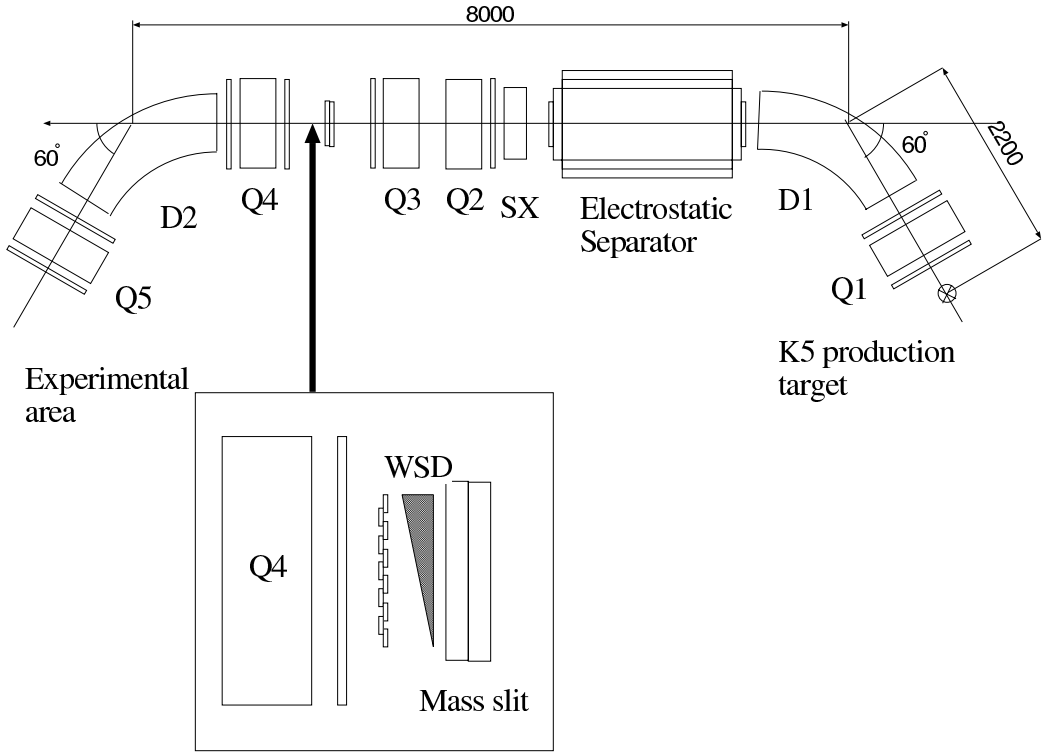

Figure 1: K5 beam line and WSD.

3 Current Analysis Progress

3.1 Calculation of Stopped Kaon Number

Yield optimization of stopped kaon is one important subject for the preparation of the main run. We have 3 components to optimize, namely, beam line setting, WSD, and degrader thickness before target. Optimization of beam line is done so as to maximize incident kaon number.

They had been done with a dedicated setup shown in Fig. 3(left). We have used a set of 10 plastic scintillators(range stack), to check stopped kaon density distribution. "K stop" is identified with the pulse-height correlation between i-th counter and (i+1)-th counter. Fig. 3(right) shows the correlation between second and third counters for K^+. Roughly speaking, they can be separated into 3 groups. First group is the set which stopped before third counter(and the decay product hits the counter). Second group is the set penetrating the third counter. The third group is the set of real stopped events("K stop").

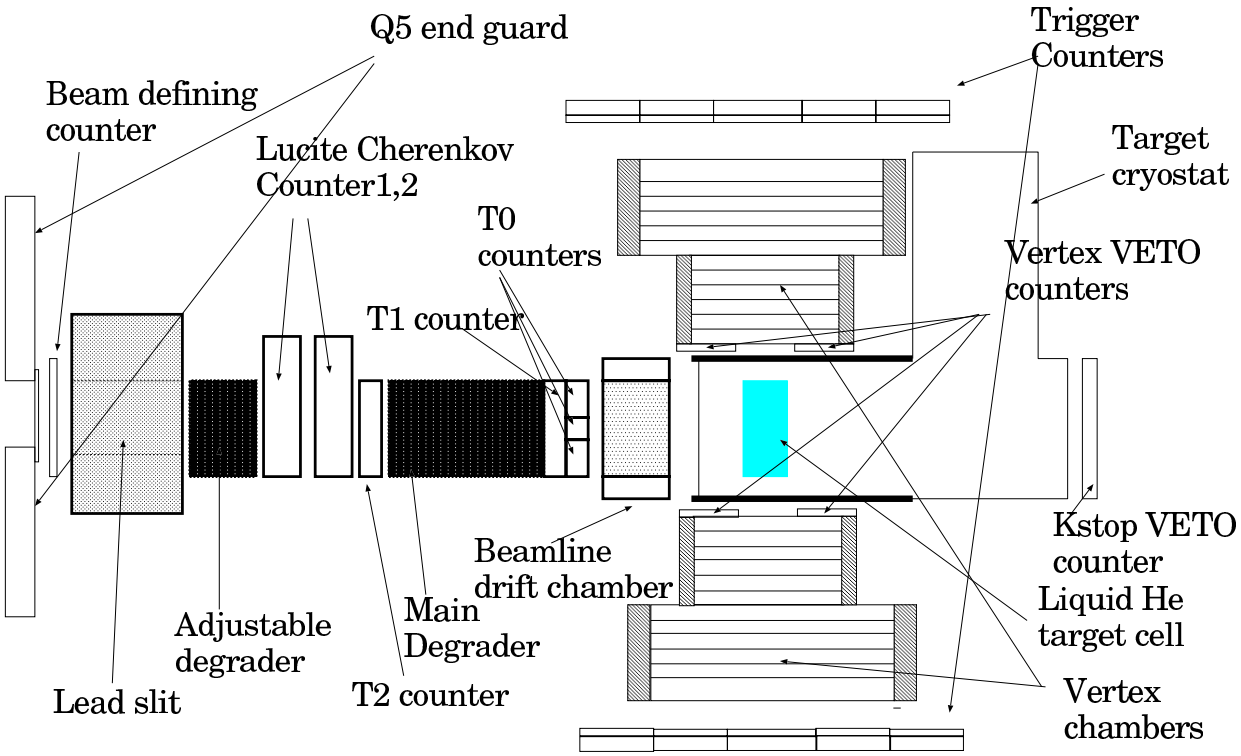

Figure 2: Conceptual view of experimental setup.

After the optimization both with and without WSD, we compared stopped kaon yield for two cases.

Fig. 4 shows maximum stopping density(i.e. number of stopped K in 1g/cm^2), between with WSD and without WSD. We can see higher density distribution with WSD, because of sharper momentum bite of kaon(left). We could obtain 1.5 times larger stopped kaon yield with WSD.

3.2 Stopped K Event Selection

A part of injected kaons into the target may react in-flight. This in-flight reaction component appears as background at higher momentum side in the neutron momentum spectrum(Because it gives small neutron time-of-flight as the result of small flight time of K^- from T0 to stopped point), and the rejection is indispensable, also for the determination of neutron TOF origin(electrical offset) described later.

In the analysis of the experiment, first selection with light quantity(defined as $\sqrt{phl \times phr}$, where *phl* and *phr* are pulse height at PMT left, and PMT right, respectively) of T0 counter(placed at most down stream) is applied to events((Fig. 5 left). This first selection corresponds to picking up kaon with momentum which can stop in 0.75g/cm^2 ^{4}He.

In fact, there exist component which cause in-flight reaction in shallow depth, even if they have small momentum enough to stop deeper position. Thus, second selection is applied with the correlation between reaction point(which is approximated with the

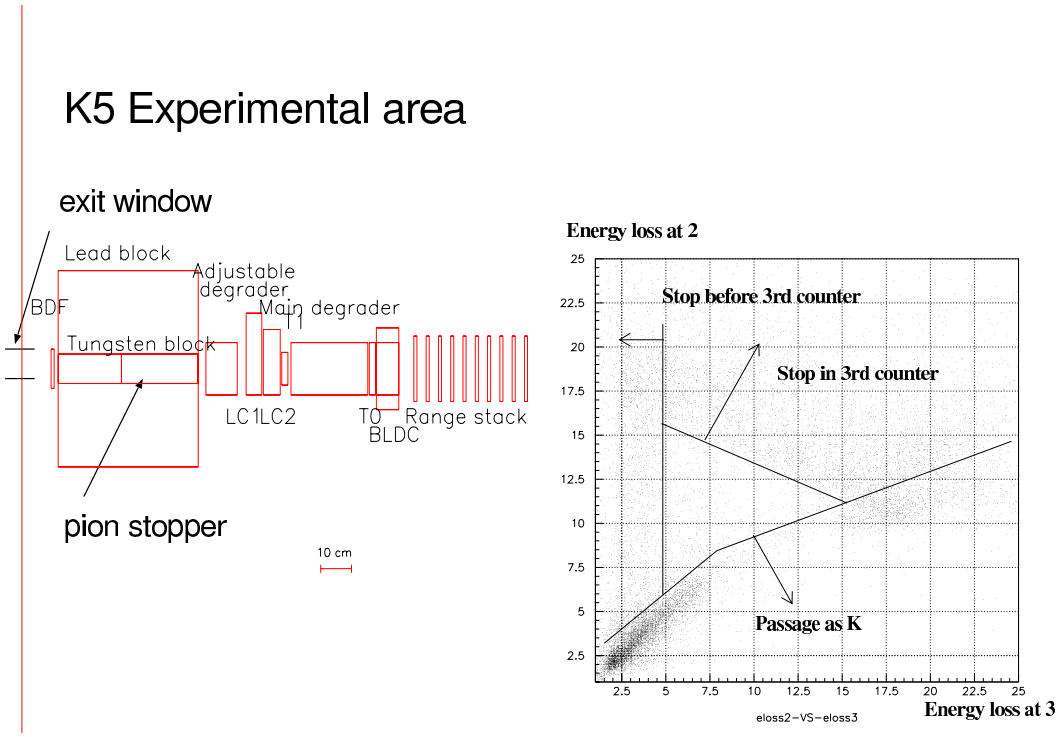

Figure 3: Schematic side view of range measurement(left), and correlation between pulse heights(right, MeVee unit) in second counter(vertical) and in third counter(horizontal).

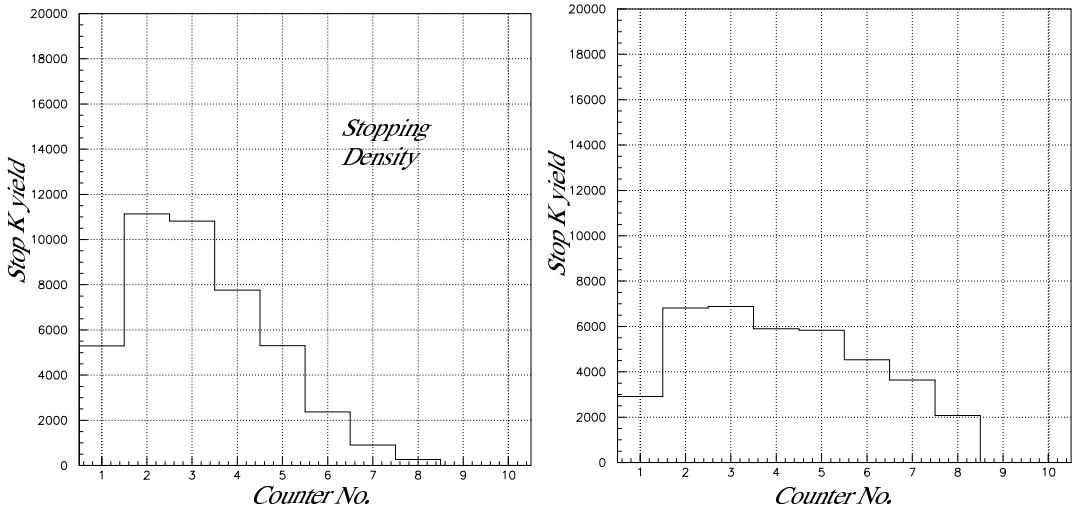

Figure 4: Comparison of density distribution for positive polarity(i.e. for K^+). Left figure shows that with WSD, and the right shows that without WSD. Vertical axis is normalized with incident proton number to the K5 production target. We can see sharper distribution for the case of with WSD. We adjusted the thickness of adjustable degrader so as to have maximum stopping density at around 3rd counter.

reaction vertex) and light quantity in T0(Fig. 5 right).

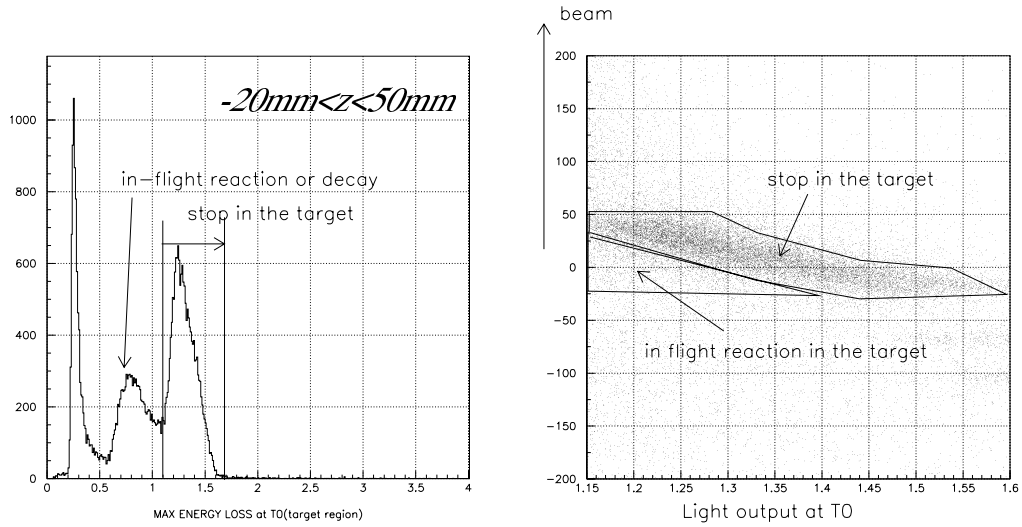

Figure 5: Light quantity distribution of T0. Right figure is the scatter plot between light quantity at T0(abscissa) vs reaction point along beam axis(ordinate, mm unit). A peak from stopped K trigger exists around relative light quantity 1.15. We can see target shadow from -20 to 50mm(right).

3.3 Track Reconstruction of Secondary Pion with Vertex Drift Chamber(VDC)

3.3.1 Track determination procedure

Incident kaon has been tracked with conventional planer type drift chamber(BLC). Because secondary π from stopped K distributes isotropically, vertex detector must have high resolution for particle with large incident angle to its sensitive planes. From such a viewpoint, hexagonal cell structure has been adopted as the vertex detector(Fig. 6 left). This hexagonal cell structure is held by feed through. This cell structure is not conventional planer type drift chamber, so that we have developed the following analysis procedure.

As the track reconstruction, approximation of cylindrical electric field is used. When N wires give hit, χ^2 is defined as:

$$\chi^2 \equiv \sum_{i=1}^{N} \frac{(\Delta r_i - \frac{|z_i - a y_i - b|}{\sqrt{1+a^2}})^2}{\sigma^2}$$

where, Δr_i is drift length to i-th hit wire, (y_i, z_i) is coordinate of hit wire, (a, b) are slope and intercept, and σ is the resolution. a and b are determined so as to minimize the χ^2.

Same procedure is applied for x-y plane. At current stage, 250μm of position resolution has been achieved.

3.3.2 Determination of time to drift-length conversion function

High accuracy is required to the time to drift-length conversion function to fulfill the required position resolution to the vertex detector. The functions are prepared separately for each wires, and they are determined by:

$$\Delta r(t) = L \frac{\int_{t_i}^{t} f(t)dt}{\int_{t_i}^{t_f} f(t)dt},$$

where, t is drift time(TDC count), t_i, t_f is initial and final point of the time distribution, and $f(t)$ is the time distribution function which is acquired from cosmic ray data independently. L is dimension of drift cell in case it is approximated by cylinder, and it is selected so as to achieve best position resolution in current status.

A typical time distribution and conversion function for the distribution are shown in Fig. 6(right).

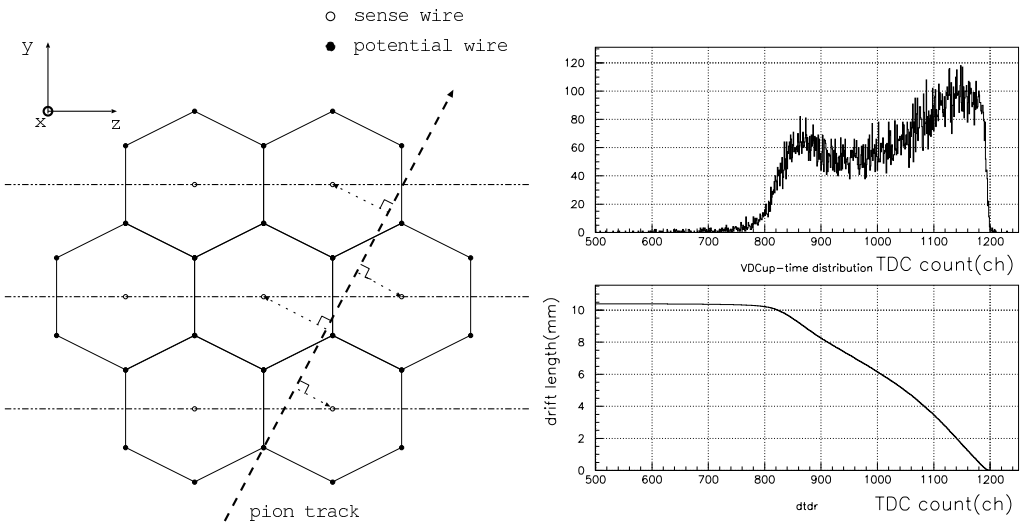

Figure 6: Circumstances of tracking of vertex drift chamber(left), and typical time distribution and time to drift-length conversion function for the distribution(right). By approximational cylindrical symmetry of the electric field, drift time is thought to be determined by the avalanche drifts from the closest approach between wire and the track.

3.4 Current Status of DCA Resolution

We construct reaction vertex with 2 straight line obtained with 2 kinds of drift chambers(VDC and BLC). Then, Distance of the Closest Approach(DCA) is defined for 2 straight lines.

Fig. 7 shows DCA distributions for K^+ and K^- at current stage. The distribution for K^- is expected to have longer tail compared with K^+ case because of Λ generation though that for K^+ is expected to be $\delta(0)$(no multiple scattering and with ultimate position resolution). Because both track of incident K and secondary π are used for the

determination of the DCA, we also need to improve both position resolutions. We need to resolve the ambiguity of relative position of both detectors so as to have better DCA resolution. Currently, 150μm and 250μm have been obtained, as the position resolutions

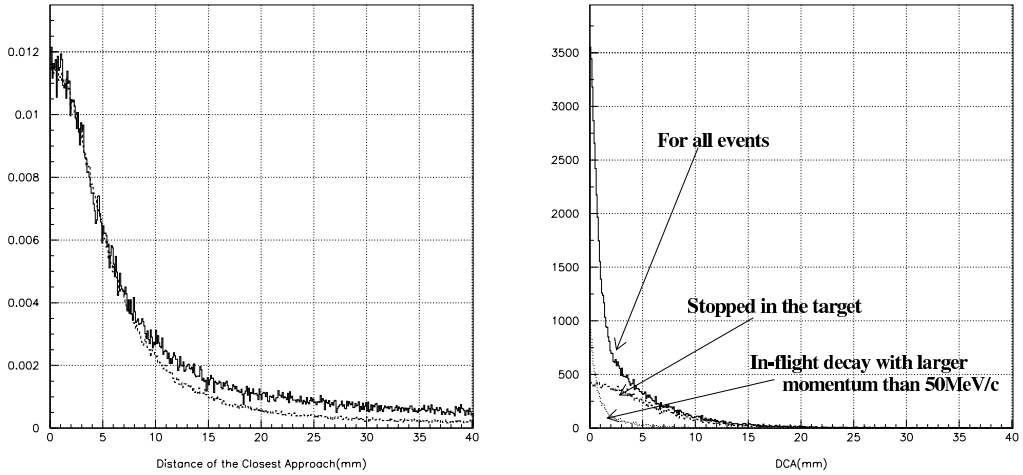

Figure 7: Comparison of DCA distributions between K^+(dot line) and K^-(solid line) at current stage(left). Distribution for K^- has long tail as the result of Λ generation. Right figure shows simulated DCA distribution for realistic setup for K^+ with GEANT3.21. Chamber resolutions and relative position ambiguity are not taken into account. Multiple scattering effect is rather large for stopped events.

of incident and secondly particle trajectory, respectively. This gives 5mm resolution for DCA.

3.5 Determination of Neutron Velocity and Current Status of Its Resolution

Neutron velocity β_n is determined with Time-Of-Flight(TOF) and the flight distance. To get both quantities, PMT's are attached to both edges of neutron counter(index up and down). TOF determination is performed along the following processes.

Firstly, quantity

$$TOF = \frac{NCTIME_{up} + NCTIME_{down}}{2} - \frac{T0TIME_l + T0TIME_r}{2}$$

is calculated. Where, $NCTIME$ is time difference between discriminated signals from PMT attached to neutron counter and T1 counter. $T0TIME$ has same meaning.

This quantity primary gives neutron TOF, but it also contain several error caused by following reason:

Determination of TDC offset Each TDC channels, and signal cables are slightly different. It appears as a offset of TDC data.

Correction of pulse-height to rise-time correlation on neutron counter(slewing correction) Light quantity of neutron inside scintillation counters have broad distribution, and the variation of TOF due to the rise-time can be corrected using pulse heights recorded in ADC's..

Correction of stopped position to travel-time correlation inside target Kaons travel 25∼30cm from T0 counter until stopping in the target. Higher momentum kaon stops deeper in the target. Therefore, kaon momentum and stopped position along beam axis are strongly correlated, and calculation of its flight time is possible.

Neutron flight distance is calculated with up-down time difference and center of closest approach points on kaon and pion tracks. Because time difference is calculated after slewing correction, slewing correction plays an important role for β_n resolution.

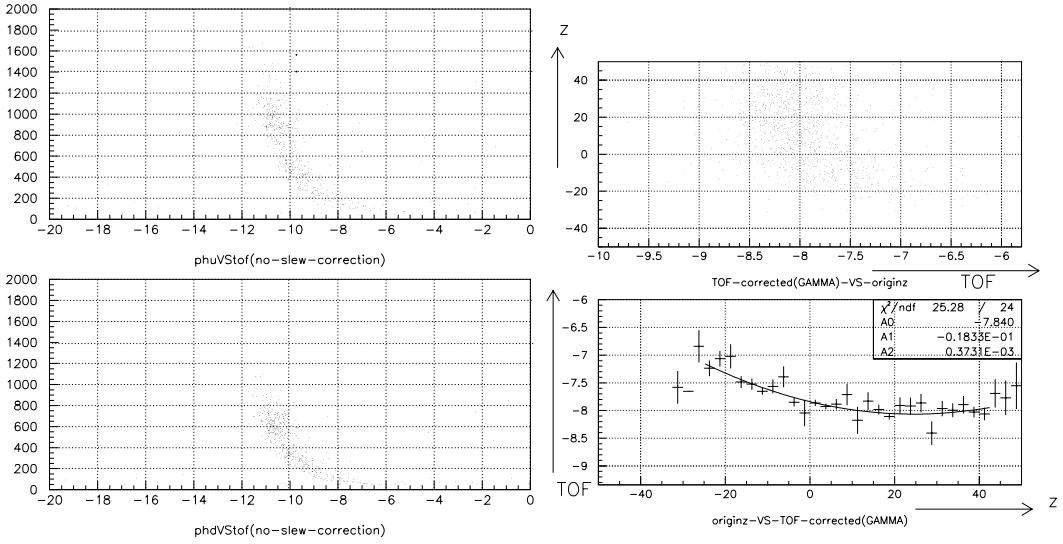

Figure 8: Pulse-height to time correlation on a neutron counter(left), (beam axis component of)stopped position-time correlation(upper-right) and its profile and fit result with second order polynomial. We can see increasing TOF to shallower depth as stopped position-time correlation.

These two correlations and offset can be removed by using γ-ray events from stopped K^- [1]. Fig. 8 shows each correlations for γ from stopped K^-.

After these correlations, β resolutions of γ is currently about 0.045 at the mean distance of 2.3m.

3.6 $\gamma - n$ Separation in $1/\beta$ Spectra and Constant Background

Fig. 9 shows $1/\beta_n$ spectra for 10% of whole statistics. We can see good $\gamma - n$ separation. Left figure is for 5MeVee threshold cut, and the right is for 10MeVee threshold cut. Accidental background appears as almost constant in $1/\beta$ spectra. We can improve

[1] γ event is picked up by the requirement of sequential hit to 3 neutron counters.

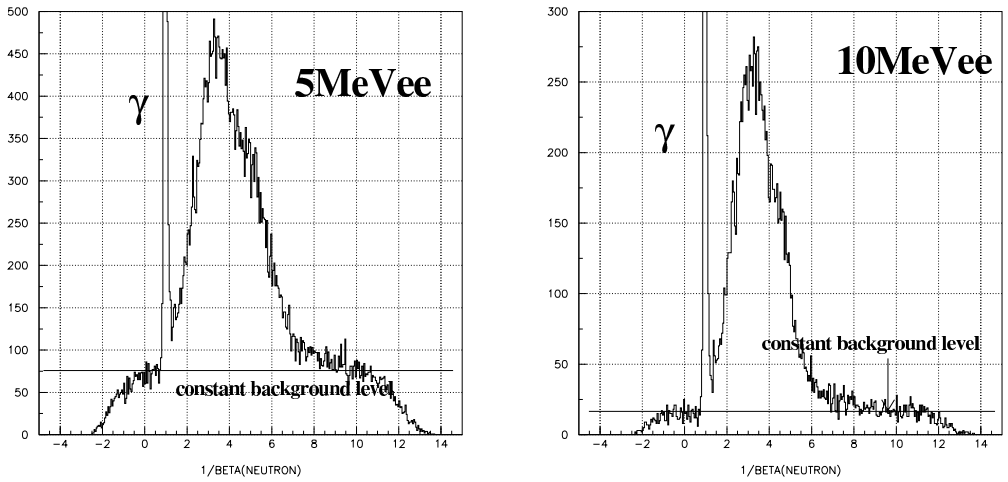

Figure 9: $1/\beta_n$ spectra in case of 5MeVee(left) and 10MeVee energy threshold. We can see a substantial improvement of S/N ratio by raising threshold level.

S/N ratio substantially by increasing energy threshold. However, if we apply higher threshold, the neutron detection efficiency get smaller especially for lower momentum neutron.

3.7 Neutron Momentum Calibration with $\Sigma^{\pm}_{stopped} \to n\pi^{\pm}$ Decay

We have mono-energetic neutrons generated by

$$\Sigma^{\pm}_{stopped} \to n\pi^{\pm}$$

which gives peaks in momentum spectra at 185.02MeV and 193.09MeV respectively. The peak caused by stopped Σ^+ is larger in yield and it is very important as unique calibration peak for the neutron momentum spectra[2].

Decay products from stopped $\Sigma^{\pm}$ are expected to go opposite direction. As shown in Fig. 10, we can observe peak caused by stopped Σ^+. This spectra are obtained by analyzing hit pattern on neutron counters and picking up events, in which neutral particle and charged particle are detected in opposite side.

If some offsets still remain, the peak doesn't appear where we expected. Thus, there is no large systematic error to deduced neutron momentum.

Note that this neutron momentum spectra are obtained with "back-to-back requirement of charged particle and neutral particle". Improving the accuracy of the event selection is a future subject.

4 Future Subjects

As farther subjects of the analysis, we can summarize as follows.

[2]Peak at 193.09MeV is expected to be weak because of the absorption.

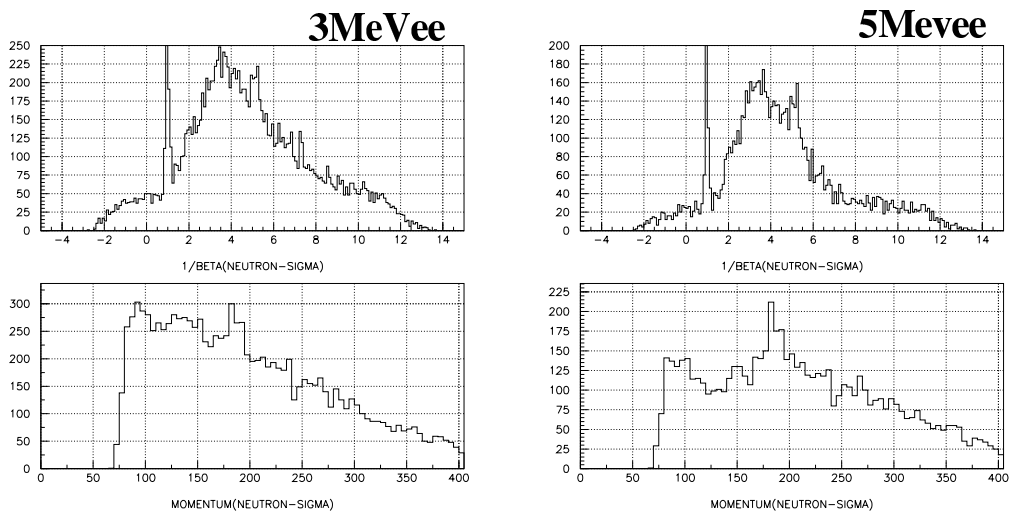

Figure 10: $1/\beta_n$(up) and momentum spectra(down, MeV/c unit) for stopped Σ-decay event, for 3MeVee threshold(left) and 5MeVee threshold(right). We can observe a peak structure around 185MeV/c for both case.

- Stability check of position resolution of MWDC throughout production runs.
- Improvement of time to drift-length conversion function for VDC
- Improvement of DCA resolution by accurate determination of relative position between BLC and VDC's.
- Determination of better correction function and coefficient for neutron counters, especially for low pulse height component.

References

[1] T.Hatsuda and T.Kunihiro, Phys. Rep. 247(1994) 241.

[2] Y. Akaishi and T. Yamazaki, Phys. Rev. C65 (2002) 044005.

[3] M. Iwasaki *et al.*, Nucl. Inst. Methods **A473** (2001) 286.

[4] K.H. Tanaka *et al.*, Nucl. Inst. Methods **A363** (1995) 114.